2004

Characteristics of a laser driven micropump

Huseyin Cagatay Yalcin
Lehigh University

Yalcin, Huseyin Cagatay

Characteristics of a Laser Driven Micropump

January 2004

Characteristics of a Laser Driven Micropump

by

Huseyin Cagatay Yalcin

A Thesis

Presented to the Graduate and Research Committee

of Lehigh University

in Candidacy for the Degree of

Master of Science

in

Mechanical Engineering

Lehigh University

(January 2004)

This thesis is accepted and approved in partial fulfillment of the requirements for the Master of Science

December 02, 2003
Date

Dr. Sudhakar Neti, Thesis Advisor

Dr. Daniel Ou-Yang, Thesis Advisor

Dr. Herman Nied, Chairperson of Department

Acknowledgments

I want to express my thanks to my advisors Prof. Sudhakar Neti and Prof. H. Daniel Ou-Yang, for their continuous support. Besides that I appreciate Prof. Alparslan Oztekin and Larry Hough for a lot of useful discussions and valuable help with the details of the thesis.

I also wish to thank to my family for their support and to my fiancée for her encouragement. Thanks are also due to my friends for all their contributions and support.

Table of Contents

List of Tables

Page

List of Figures

Page

ABSTRACT

Transport of fluids in micro-electro-mechanical systems (MEMS) and bio systems is quite important. Pumping of the fluid can be achieved in many ways such as by mechanical, electromechanical and an optical means of fluid transport, which is presented here. Design and analysis of a laser driven micropump is discussed in that study. Liquid transport is achieved by exerting laser force onto the particles in the liquid. The laser energy is coupled into a 50 μm hollow glass fiber/tube (microchannel). As the beam is focused into channel, the photons exert a force onto the particles in the liquid inside the microchannel. Particles are accelerated through the microchannel and they drag the surrounding fluid with them. Several other types of micropumps are also analyzed to be able to compare the performance of this micropump with others. Theoretical Particle velocities calculated based on theory are compared with experimental measured particle velocities to verify the validity of the experimental technique. Flow rate in the microchannel is calculated for different particle sizes and laser powers to bring out the parametric variations.

INTRODUCTION

The application of micro-electro-mechanical systems (MEMS) technology to micro-fluidic devices, such as micro-electronic cooling systems and bio-analytical systems, has spurred the development of micropumps to transport a variety of fluids for a wide range of flow rates and pressures. In this study, design and performance of a novel micropump is analyzed. In this design, the driving forces of photons in a laser beam are used to transport particles in the fluid to pump the fluid.

Most micropumps used today can be classified into two main categories: These are, membrane-displacement micropumps and field-induced flow micropumps [1-2]. In membrane displacement micropumps, the deflection of a microfabricated membrane provides the pressure work for the pumping of liquids. Membrane micropumps may be further classified based on how the membranes are actuated and these include piezoelectric micropumps, electrostatic micropumps, thermopneumatic micropumps and electromagnetic micropumps [1-2].

In field-induced micropumps, an external field, like electric or magnetic field, provides the pressure work for the pumping of liquids. Field induced micropumps include electroosmotic micropumps, electrohydrodynamic micropumps, magnetohydrodynamic micropumps and bubbles in flow micropumps [1-2] .The micropump design presented here can be counted among latter category since it uses laser scattering force as the driving force but on suspended particles.

In the micropump presented here, the working fluid is dragged through a microchannel by the motion of spherical particles driven by radiation forces exerted

by a laser. The idea of translating and transporting the particles with laser force is not new. In 1970, Ashkin showed that one could use the forces of radiation pressure of photons from focused laser beams to significantly affect the dynamics of small transparent micrometer sized neutral particles. Two basic light pressure forces were identified: a scattering force in the direction of incident light beam, and a gradient force normal to the beam along the intensity gradient of the beam [3]. It was shown that, with these forces, one could accelerate, decelerate, and even stably trap μm sized particles [4]. Over the years, these newly found laser trapping and manipulation techniques have been applied to a wide range of particle types, including particles as diverse as atoms, molecules, submicron particles, and macroscopic dielectric particles hundreds of micrometers in size. Even living biological cells and organelles within cells can be trapped and manipulated without optical damage.

Optical manipulation techniques have found some interesting applications especially in the biotechnology area. Many researchers have studied transport phenomena in cells with these techniques. Additionally coupling laser light into hollow fibers has made it possible to transport the cells over relatively long distances. Odde [5], managed to manipulate and deposit biological materials on surfaces with millimeter accuracy with this technique by using hollow optical fibers. He called this process, "Laser Guided Direct Writing" and made good advances toward three-dimensional cell patterning in tissue engineering.

In the present study, laser forces are used to transport fluids by exerting radiation pressure on solid particles in the fluid. Laser beam is coupled into a hollow

fiber that allows particles to be transported over longer distances than is possible with tightly focused beams. The present study also includes theoretical calculations of pressure forces on the particles using generalized Lorenz-Mie theory and particle and fluid velocity calculations using Stoke's drag equations and Habermann exact theory.

The experiments were observed through an inverted microscope. Laser light scattered by small silica particles made it possible to locate the otherwise invisible IR laser beam. Laser light scattered by the larger polystyrene particles made it possible to locate the position of the polystyrene particles. Motions of the polystyrene particles were projected onto a CCD camera, and the images were recorded onto an S-VHS videocassette recorder. The recorded images were analyzed frame by frame Global Lab Image Software from Data Translation Inc., to determine the velocities of the polystyrene particles.

The rest of this thesis is organized as follows. First, various types of micropumps are described followed by an explanation of the scattering phenomenon. After that, the theory behind the flow calculations is discussed. The following chapters deal with experimental technique, theoretical results and experimental results. Finally, the quantitative performance of the micropump is presented and a brief conclusion is given at the end.

Chapter 1

Basics of Micropumps

Development of micropumps has been spurred by the application of micro-electro-mechanical technology to microfluidic devices, such as micro-electronic cooling systems and bio-analytical systems. Micropumps have been used to transport a variety of liquids over a wide range of flow rates and pressures. Micropumps can be classified into two groups: membrane-displacement pumps and field-induced flow pumps. Some basic aspects of micropumps are described below.

1.1 Membrane Displacement Micropumps

In membrane displacement pumps, the deflection of the microfabricated membranes provides the pressure work for the pumping of liquids. Membrane pumps may be further classified based on how the membranes are actuated, including piezoelectric, electrostatic, thermopneumatic and electromagnetic micropumps [1-2].

High flow rates are achievable with these pumps and also many types of liquids can be pumped. The flow produced is pulsed rather than continuous. The major disadvantage is that they require some moving parts, such as check valves, which complicates the fabrication and operation. The moving parts can get contaminated or damaged which could shorten the lifetime of the pump. A membrane displacement pump is shown schematically in the figure below:

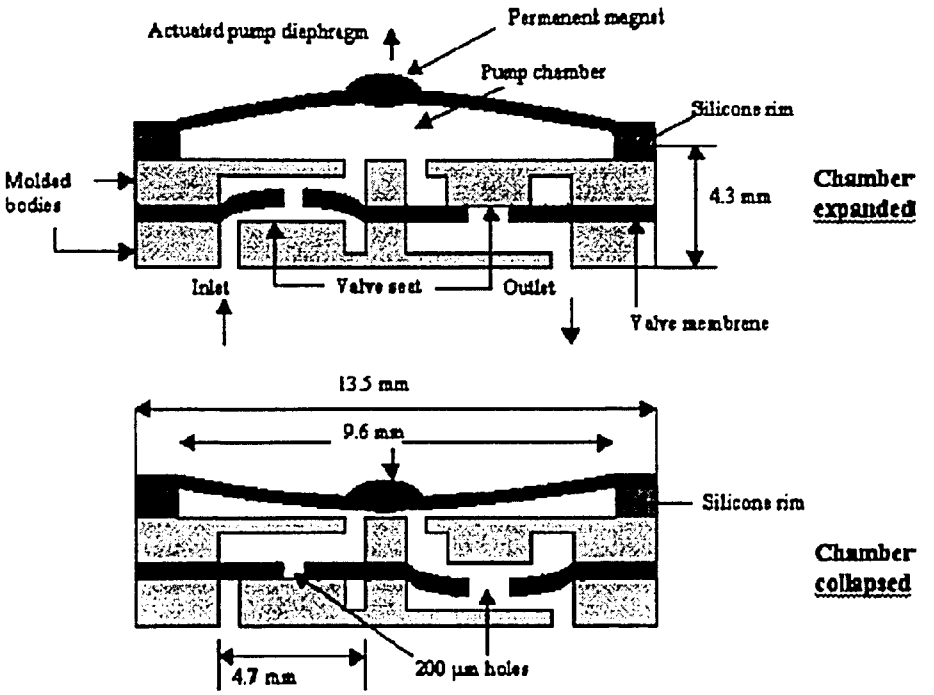

Figure 1.1 A Membrane Displacement Pump

The pump in the figure has been fabricated and tested by a group in University of Florida [6]. The membrane of the pump is magnetically actuated and the pump is 15 mm in diameter, 20 mm long and weighs about 10g. Pumping is achieved with the operation of the valves at 600 Pa pressure differentials. Change in the flow rate with pressure difference for this pump for pumping water is shown in the figure below:

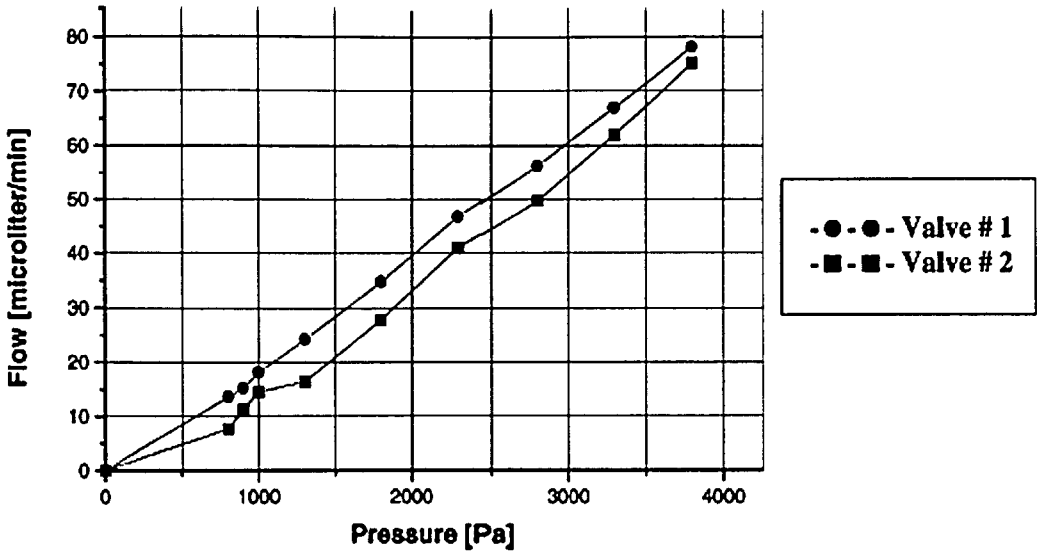

Figure 1.2 Flow Rate vs. Pressure Differential for two One-Way Valves for the Magnetically Actuated Membrane Displacement Micropump

In this figure, valve #1 is the inlet valve and valve #2 is the outlet valve. Differences in the flow rates through the two valves are attributed to the small differences in the manual manufacturing processes of the valves. As seen from the figure, maximum flow rate of about 75 μlt/min is achieved at about 3,750 Pa. The amount of power consumed at the maximum pumping rate is about 1.9 W.

1.2 Field Induced Micropumps

Field induced micropumps use an external field, such as an electric or a magnetic field to provide the pressure for the pumping of liquids. Field induced micropumps can be divided into electroosmotic micropumps, electrohydrodynamic micropumps, magnetohydrodynamic micropumps and bubbles in flow micropumps depending on the forces used [1-2]. The micropump model developed as part of this work uses the idea of pumping the fluids with laser driven particles and can also be counted in this category of micropumps.

When compared to membrane displacement pumps, field induced pumps usually do not create as high flow rates as displacement devices. But a clear advantage of field induced micropumps is that, they do not require moving parts such as check valves, which simplifies the fabrication and operation. This makes it possible to fabricate pumps with very small dimensions. Unlike membrane displacement pumps where the flow is pulsed, in field induced pumps the flow is usually continuous. Basic features of these micropumps are explained below.

1.2.1 Electroosmotic Micropumps

Electroosmotic micropumps use field induced ion drag to drive liquids and achieve high pressures in a compact design with no moving parts. Electroosmotic pumping is the motion of bulk liquid caused by the application of an electric field to a channel with a charged wall. Most surfaces spontaneously acquire a finite charge density when in contact with an aqueous solution [7]. In the case of contact between

glass (or silica) and an aqueous electrolyte liquid, the glass surface becomes charged due to deprotonation of surface silanol groups. The charged surface attracts counter-ions and repels co-ions. If an external electrical field is applied parallel to the dielectric wall, Coulombic forces are exerted on the mobile ions in the net positive layer above the shear plane and the electromigration of these ions forces the bulk liquid motion through viscous interaction. The principles of this type of micropump can be understood from the figure below:

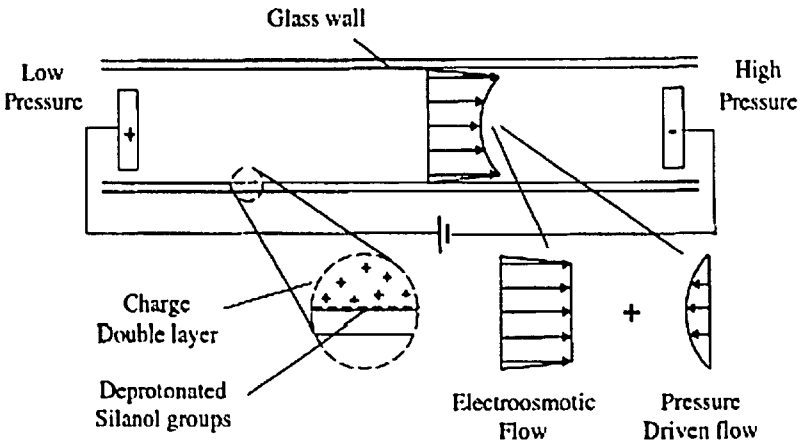

Fig 1.3 Basic Flow Principle of Electroosmotic Micropumps

In addition to high pressure capacity, electroosmotic pumps have one other major advantage over other field induced pumps. These pumps can pump working fluids of a wide range of conductivity including organic solvents, deionized water and high-conductivity aqueous solutions.

A schematic of an electroosmotic micropump is shown in the figure below:

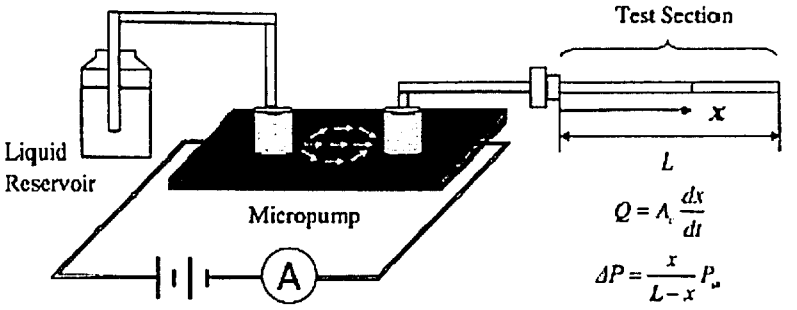

Fig 1.4 An Electroosmotic Micropump

The pump in the figure has fabricated and tested by a group in Stanford University [7] with approximate dimensions of 38 mm x 1 mm x 0.9 μm. The working principle and measurement techniques are quite simple. When high voltage is applied, the electroosmotic micropump drives working fluid from the outer liquid reservoir to the test section. The test section is composed of circular silica capillary with an inner diameter of 700 μm. For an open test section tube, maximum flow rate is measured by tracing the flow front. When the test tube is closed, both flow rate and counter pressure are measured simultaneously. Change in the flow rate with pressure for that pump in the case of pumping deionized water, is shown in the figure below:

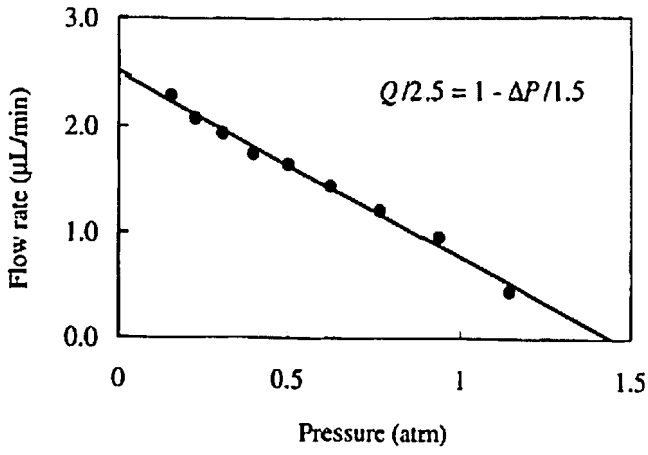

Fig 1.5 Flow rate vs. Pressure for the Electroosmotic Micropump

The above data are from an experiment with a 3 kV potential, which is the maximum voltage that could be applied, and 7 μA current. The maximum flow rate is about 2.5 μlt/min and maximum pressure capacity is about 1.5 atm.

1.2.2 Electrohydrodynamic Micropumps

In electrohydrodynamic pumping, fluid forces are generated by the interaction of electric fields and charges in the fluid. This interaction yields a force on the charge, which then transfers momentum to the fluid. To enable the existence of free charge, a spatial gradient in the conductivity in the medium is necessary. The most common way to create spatial gradient in the conductivity is to make a temperature difference in the slightly conducting liquid. The electrical conductivity of slightly conducting liquids often depends strongly on the temperature, most often increasing with increasing temperature. Hence by developing a temperature gradient in the liquid, a

gradient in electrical conductivity can also be obtained [8]. This type of micropump can be shown schematically as below:

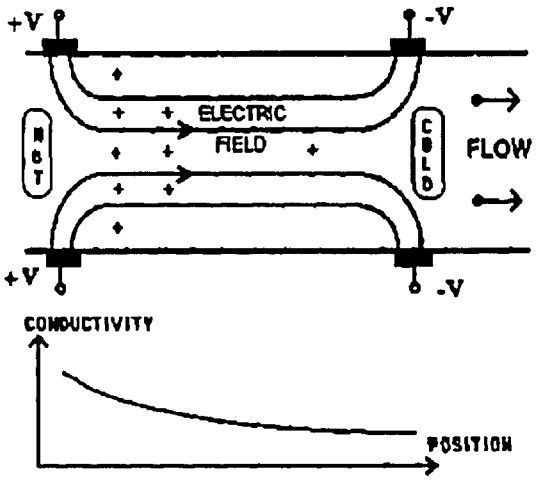

Fig 1.6 Basic Flow Principle of Electrohydrodynamic Micropumps

For this configuration, the region labeled "HOT" might be obtained by fabricating resistors in the walls of the flow channel or by suspending them across the channel itself. The longitudinal temperature gradient and consequent conductivity gradient allows free charge to develop in the fluid volume. This charge is then acted on by the longitudinal electric field to yield a pumping force [8].

The major disadvantage of electrohydrodynamic micropumps is that aqueous solutions cannot be pumped with these pumps due to their high ionic conductivity, and thus the use in medical or biological systems is restricted [8].

An electrohydrodynamic micropump was fabricated and tested by a group in Fraunhofer-Institute for Solid State Technology in Munich [9]. With approximate

dimensions of 3 mm x 3 mm x 30 μm. Change in the pressure with flow rate, change in the flow rate with voltage, and change in the flow rate with pressure for pumping ethanol, is shown in the figures below:

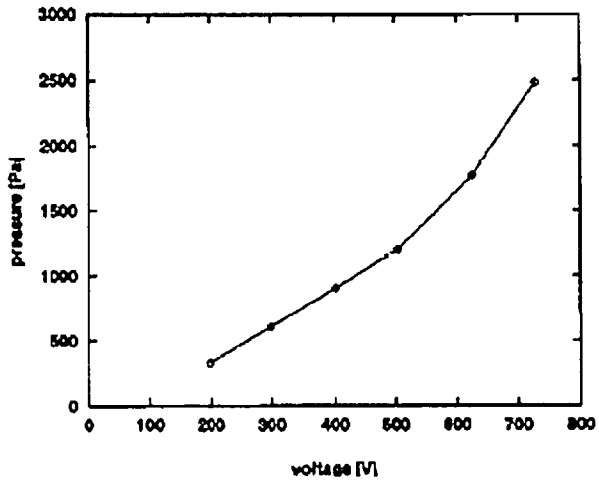

Fig 1.7 Pressure vs. Voltage for the Electrohydrodynamic Micropump

The above figure shows the pressure generated at zero flow rate as a function of the applied voltage. A maximum pressure of 2,480 Pa is achieved with a driving voltage of 700 V.

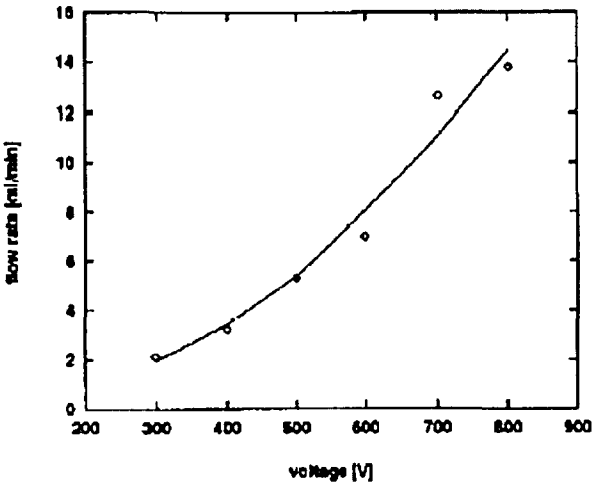

Fig 1.8 Flow rate vs. Voltage for the Electrohydrodynamic Micropump

In the above figure, the flow rate is depicted as a function of the applied voltage at a constant pressure head of 420 Pa. A maximum flow rate of 14 ml/min was achieved in this device.

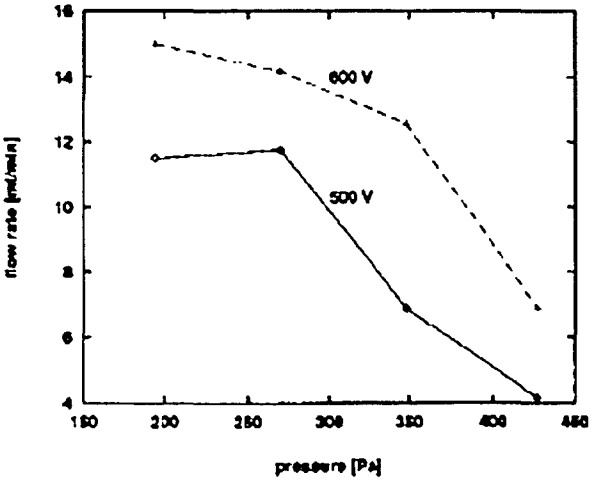

Fig 1.9 Flow rate vs. Pressure for the Electrohydrodynamic Micropump

The above figure shows the flow rate versus pressure for two different driving voltages of 500 V and 600 V respectively for the flow of ethanol in the 30 μm channel/pump.

1.2.3 Magnetohydrodynamic Micropumps

The pumping mechanism for a magnetohydrodynamic pump is a result of the Lorentz Force. This force is produced when an electric current is applied across a channel filled with conducting solution in the presence of a perpendicular magnetic field. The Lorentz Force is both perpendicular to the current in the channel and the magnetic field [10]. Principle of this type of micropump can be better understood from the figure below:

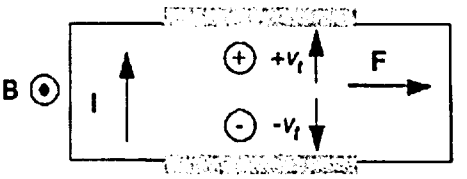

Fig 1.10 Basic Flow Principle of Magnetohydrodynamic Micropumps

The above figure is top view of a magnetohydrodynamic micropump. The magnetic field, which is represented with B, is out of the page. I, stands for the electric current and the direction of the electric current is from the bottom to top. F is the Lorentz Force and for this configuration its direction is towards right.

Magnetohydrodynamic micropumps are suitable to pump high conductivity liquids. So these pumps are widely used in medical and biological applications.

A magnetohydrodynamic micropump was fabricated and tested by a group in Pohang University of Science and Technology, South Korea [10]. The pump is 800 μm x 380 μm x 4 mm. The micropump could pump NaCl solution at maximum flow rate of 18.3 μlt/min while consuming about 2W of power.

1.2.4 Buble in Flow Micropumps

Although there are several different types of bubble micropumps, the one, which will be discussed here is a thermal buble- actuated micronozzle-diffuser micropump [11]. The working principle of the micropump is liquid/vapor phase transition with nozzle/diffuser flow regulation. The micropump consists of a resistive heater, a pair of nozzle-diffuser flow controllers and a 1 mm in diameter 50 μm in depth pumping chamber. Pumping principle is illustrated in the following figure:

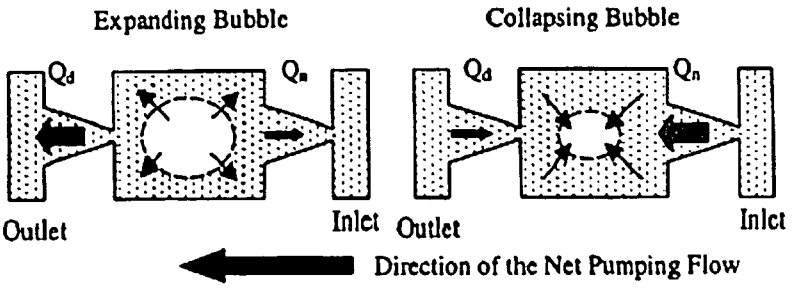

Fig. 1.11 Pumping Principle Illustrated from the Top View of the Pumping Chamber for the Buble in Flow Micropump.

A bubble is generated in the micro chamber by thermal bubble nucleation to create a pumping pressure source. As the pumping bubble expands, the volume flow rate at the diffuser, Q_d, is larger than the one at the nozzle, Q_n. When the pumping

bubble collapses, Q_d, is smaller than Q_n. This process generates a net flow from the nozzle to the diffuser.

A better schematic drawing of the micropump is shown in the figure below:

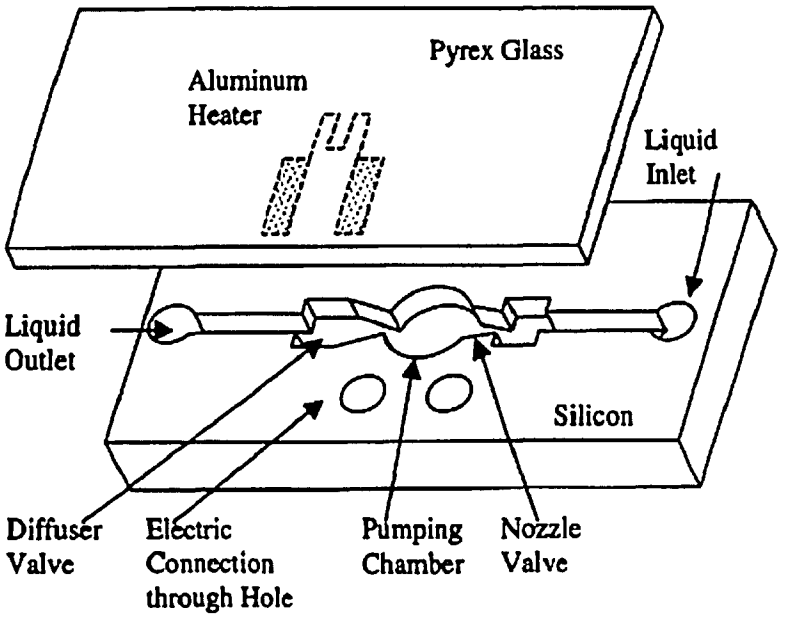

Fig. 1.12 Schematic Drawing of the Nozzle-Diffuser Based Bubble in Flow Micropump

The pumping chamber, nozzle-diffuser flow controller and channels, all are 50 μm deep. The circular pumping chamber is 1mm in diameter. The nozzle-diffuser flow controller is 30 μm at the narrow neck, and 274 μm in the open mouth. The fluid channels that connect the micropump to the fluid inlet/outlet ports are 200 μm in width.

The maximum flow rate achieved with this design is about 5 μlt/min with a static pumping pressure of above 377 Pa for zero flow conditions. Power consumption for maximum flow rate is about 1 W.

1.2.5 Laser Driven Micropump

Development and characterization of a laser driven micropump is the primary emphasis of this thesis work. The basic operation of this type of micropump can be explained as follows. When a laser beam interacts with a particle, the redirection of the light rays result in the change of momentum of the photons and this momentum is transferred to the particle. Focusing the laser with a low numerical aperture (NA) lens in the presence of a particle with a refractive index bigger than that of the medium, results in a force on the particle that attracts the particle to the beam center and pushes the particle in the laser propagation direction. The micropump in this work uses this force as the driving force. In its simplest implementation, a laser is focused toward a microchannel that is connecting two reservoirs. As the particles in the fluid are pushed from one reservoir to the other with the laser forces (through the microchannel), fluid in the microchannel is transported along with the particles. A simple schematic drawing of this micropump is given in the figure below:

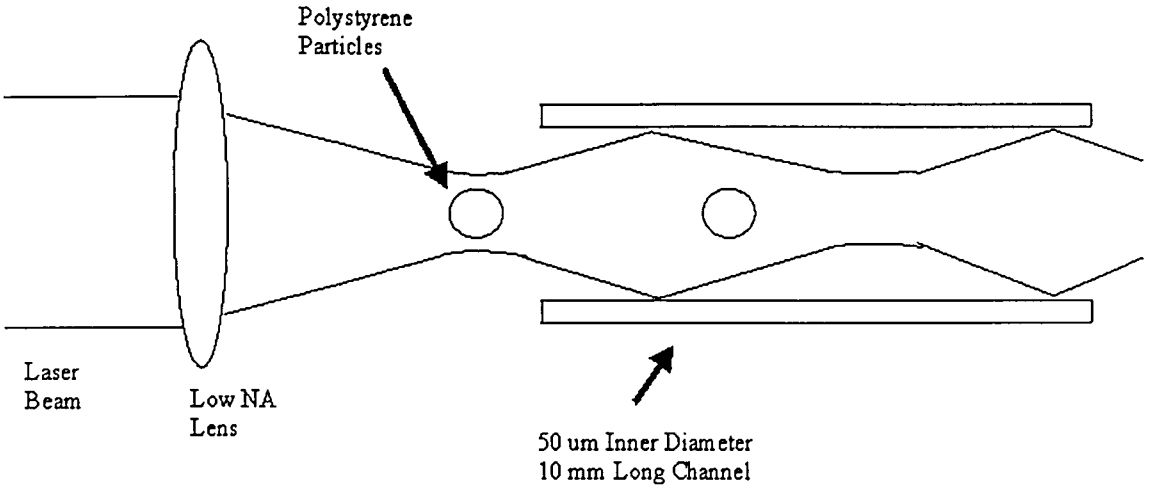

Figure 1.13 The Laser Driven Micropump

A laser driven micropump has some advantages over other field induced micropumps. Almost any type of liquid can be pumped with this micropump and the fluid can be pumped over relatively large distances since the laser exerts a continuous force on the particles in the microchannel as it proceeds through the microchannel. Detailed analysis of this micropump will be given in the following chapters.

Chapter 2

Locomotion of Particles with Laser Photons

Photons have linear and angular momentum and therefore they can exert (radiation) pressure and torque on physical objects. The forces are very small (~pico N) and are difficult to detect. But, if the light is focused with a lens or an objective and the intensity of the light is increased, then these forces could be significant. Lasers are used as high intensity sources in many optical manipulation experiments. The experiments conducted in this work could best be explained as follows: When laser light is focused through a low numerical aperture lens onto a solid particle, two basic light pressure forces are exerted on the particle arising from the interaction between the laser light and the particle. These can be identified as: (1) a scattering force in the direction of the incident light beam, and (2) a gradient force in the direction of the intensity gradient of the beam (normal to the beam). The gradient force is towards the beam center when the refractive index of the particle is greater than the surrounding medium, and it is in the opposite direction when the refractive index of the particle is smaller than the surrounding medium. The interaction between the light and the particle is stronger when the difference between the refractive indices of the particle and surrounding medium is larger. For particles with diameters larger than the light wavelength, a model based on geometric optics can be used to describe the phenomenon [12]. The reasoning behind the scattering and the gradient forces for the larger particles can be understood from the following figure:

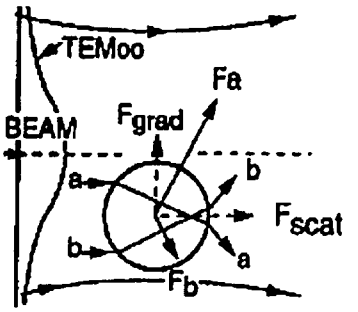

Figure 2.1 Origin of the Scattering and the Gradient Forces for a High Index Sphere Displaced from Beam Axis

In Figure 2.1, a high index of refraction sphere ($n_{sphere} > n_{medium}$), which is many wavelengths in diameter, is shown at a location off axis in a mildly focused Gaussian Beam. Consider a pair of rays "a" and "b" striking the sphere symmetrically about its center. Neglecting relatively minor surface reflections, most of the rays refract through the particle, giving rise to forces F_a and F_b in the direction of the momentum change. Since the intensity of ray "a" is higher than ray "b", the force F_a is greater than F_b. Adding all such symmetrical pairs of rays striking sphere, one sees that the net force can be resolved into two components: $F_{scat.}$, the scattering force component pointing in the direction of the incident light, and $F_{grad.}$, the gradient force component arising from the gradient in light intensity and pointing transversely toward the high intensity region of the beam. For a particle on axis or in a plane wave, $F_a = F_b$ and there is no net gradient force component. Additionally, when a low index of particle is placed off axis in the beam, refraction through the particle reverses, F_a is less than F_b and such a particle will be pushed out of the beam. To calculate the scattering and the gradient force components on the particle, effect of light on the particle should be better analyzed. The interaction of light with an object

(scattering), can be divided into two components: 1) Reflection and refraction at the surface of the particle and 2) Diffraction from the rearrangement of the wavefront after it interacts with the particle. It is important to note that the radiation pattern due to reflection and refraction emanates from the particle in all directions thus depends on the refractive index of the particle. By contrast, the diffraction pattern is primarily in the forward direction and depends only on the particle geometry, so the pattern will be same for absorbing, transparent and totally reflecting spheres. The effect of diffraction becomes smaller with increasing particle size. So, when the particle is large compared light wavelength, the behavior can be explained using geometric optics to estimate the scattering pattern due to reflection and refraction, while the diffraction effects are neglected [13].

Consider a beam of parallel rays focused to "a point", illuminating a single spherical particle. If the particle is large compared to the wavelength of incident light, the rays will be reflected and refracted at the particle surface according to geometric optics and Snell's Law. Resulting radiation force from each ray can be broken into a force parallel to the direction of each ray and a force orthogonal to the direction of each ray [12]. These forces are:

$$F_{parallel} = \frac{n_m.P}{c}\left\{1+R.\cos(2\theta)-\frac{T^2[\cos(2\theta-2r)+R.\cos(2\theta)]}{1+R^2+2.R.\cos(2r)}\right\} \tag{2.1}$$

$$F_{orthogonal} = \frac{n_m.P}{c}\left\{R.\sin(2\theta)-\frac{T^2[\sin(2\theta-2r)+R.\sin(2\theta)]}{1+R^2+2.R.\cos(2r)}\right\} \tag{2.2}$$

where

where

n_m : Refractive index of the medium

P : Power of laser

c : Speed of light in vacuum

R : Fresnel reflection coefficient

T :Fresnel transmission coefficient

θ : Angle of incident radiation

r : Angle of refraction

Interaction of these equations over all angles will result in the summing of all the forces on the particle.

As mentioned earlier, with decreasing particle size, it becomes necessary to take diffraction effects into account. The generalized Lorenz Mie Theory (GLMT) accounts for diffraction effects as well as reflection and refraction effects. The GLMT theory is essentially valid for any arbitrary particle size, refractive index and wavelength [13].

Describing a Gaussian wave properly is important in GLMT to evaluate the laser-induced forces. GLMT introduces an infinite set of beam-shape coefficients as partial wave expansions to describe the nonplane wave nature of the illuminating beam. These beam shape coefficients can be resolved with reasonable speed using an improved localized approximation [14].

GLMT can be used to predict the presence of resonances, signifying the creation of electric and magnetic multipoles in the particle. Resonance effects could

cause fluctuations in the trapping forces as a function of the wavelength and particle size. GLMT has been shown to be good at predicting resonance by Nahmias and Odde [13].

The procedure to calculate forces on a particle using GLMT is as follows: The Cartesian coordinate center is located at the beam waist center, where z is the axial direction of the beam propagation and x is the polarization direction of the electric field. The center of the particle is defined as position $\vec{r} = (x, y, z)$, and $\hat{x}, \hat{y}, \hat{z}$ are unit vectors in the *x*, *y*, and *z* directions respectively. The force vector $\vec{F}$ is then given as:

$$\vec{F}(\vec{r}) = \frac{n_m}{c}\frac{2P}{\pi(w_0)^2}\left[\hat{x}C_{pr,x}(\vec{r}) + \hat{y}C_{pr,y}(\vec{r}) + \hat{z}C_{pr,z}(\vec{r})\right] \tag{2.3}$$

where

w_0 : Beam radius at the focal point (beam waist)

$C_{pr,x}$: Pressure cross section in x direction

$C_{pr,y}$: Pressure cross section in y direction

$C_{pr,z}$: Pressure cross section in z direction

From above, the scattering force is:

$$\vec{F}_{scat.}(\vec{z}) = \frac{n_m}{c}\frac{2P}{\pi(w_0)^2}\left[\hat{z}C_{pr,z}(\vec{r})\right] \tag{2.4}$$

and the gradient force is given as:

$$\vec{F}_{grad}(\vec{r}) = \frac{n_m}{c}\frac{2P}{\pi(w_0)^2}\left\{\sqrt{(C_{pr,x})^2 + (C_{pr,y})^2}\right\} \tag{2.5}$$

The scattering force is in the direction of the incident light beam and the gradient force is in the direction of the intensity gradient of the beam.

Details pertaining the calculation of the pressure cross sections are rather complicated and are not discussed here but more details are presented by Gousbet [14].

To evaluate the scattering force and gradient force exerted by a Gaussian beam on a spherical particle, a computer program based on GLMT was used in this work. This program developed by Y. K. Nahmias and has been proven to be in good agreement with experimental results [13]. In the next few chapters, results of this program for the present experimental conditions will be compared with the experimental results.

Chapter 3

Analysis of Scattering Force

The equations described in the previous chapter will be used for the evaluation and analysis of the scattering force in this chapter. As stated earlier, the scattering force on the particle varies with the radial and axial location of the particle near (in) the beam waist (minimal beam radius at focal point), wavelength and power of laser, beam waist dimensions, refractive index of particle, refractive index of medium and particle radius. The scattering force was calculated with the computer program written by Nahmias and details of the computational procedure can be found in his work [13].

3.1 Variation of Scattering Force with Particle Location

Scattering forces for varying axial positions (beginning from the beam waist and through the laser propagation direction) are calculated from that analysis. The transverse distance is zero which means the particle is at the beam center (X =0, Y=0). Laser wavelength is 1064 E-6 m and the laser power is 1 W. The beam waist is 10 E-6 m and the particle refractive index is 1.6 while the refractive index of the surrounding medium is 1.3. For the present calculation, the radius of particle is 5 E-6 m.

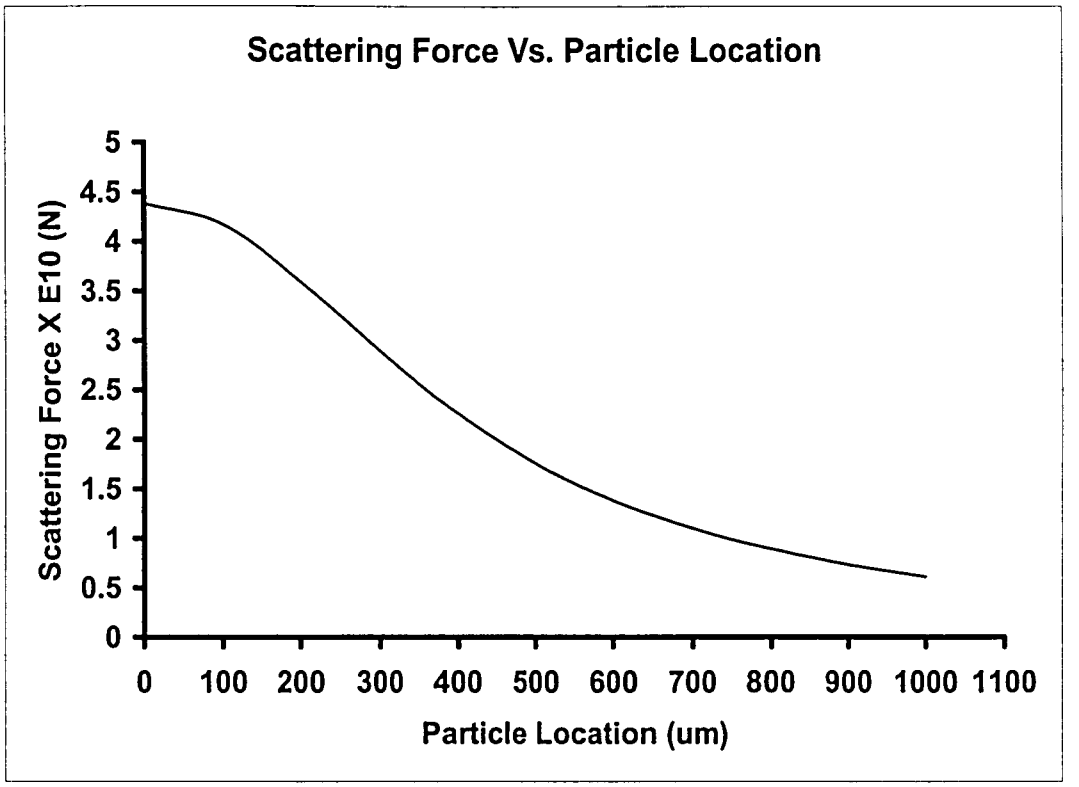

Figure 3.1 Scattering Force Vs. Particle Location

As seen from Figure 3.1, scattering force decreases continuously as the particle gets farther from the beam waist center (focal point of laser). The effective forces are about ten times smaller than the case in the focal point, when the particle is about 1 mm away from the focal point. To prevent this dramatic decrease in the scattering force as for particles farther from the focal point, laser light can be coupled into a fiber, which does not allow the laser to expand. This technique is attempted in the present work.

3.2 Variation of Scattering Force with Laser Wavelength

Scattering forces for various laser wavelengths are calculated using GLMT analysis. Particles are assumed to be at the beam center (X=0, Y=0, Z=0) with a laser power of 1 W and beam waist of 10 e-6 m. The refractive index of the particle is 1.6 and the refractive index of the medium is 1.3 and the particle radius is 5 e-6 m.

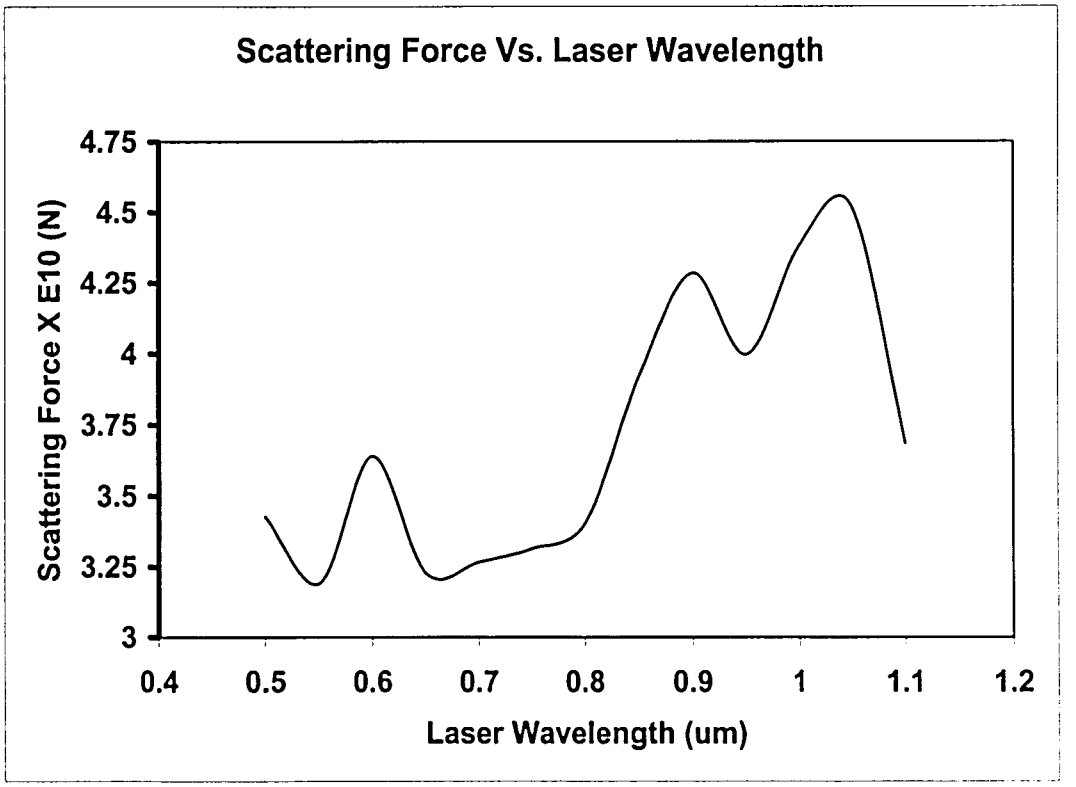

Figure 3.2 Scattering Force Vs. Laser Wavelength

As seen from Figure 3.2, larger wavelengths appear to yield larger scattering forces. The fluctuations in the scattering force with increasing laser wavelength are due to resonance effects and these effects on the scattering force are explained in detail by Nahmias [13].

The laser used for the present study is a Nd:Yag laser having a wavelength of 1.064 μm, a relatively large wavelength. So it enhances the performance of the micropump.

3.3 Variation of Scattering Force with Laser Power

Scattering forces as a function of laser power are calculated using GLMT analysis. Particles are again assumed to be at the beam center (X=0, Y=0, Z=0) with a laser wavelength of 1 e-6 m and beam waist of 10 e-6 m. The refractive indexes of the particle and medium are 1.6 and 1.3 respectively with a particle radius of 5 e-6 m.

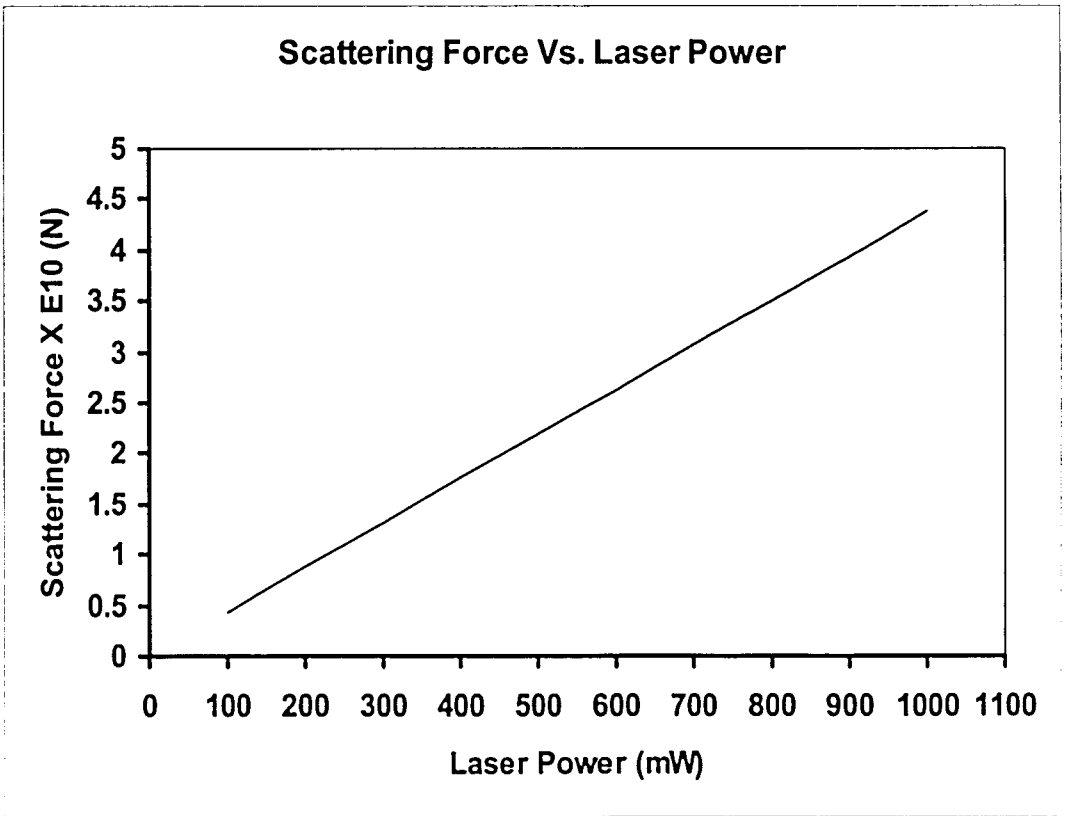

Figure 3.3 Scattering Force Vs. Laser Power

As expected, scattering force increases linearly with increasing laser power. This indicates that, it is sufficient to do the experiments at one laser power and we should be able to predict the flow behavior at other higher or lower laser powers.

3.4 Variation of Scattering Force with Nondimensional Particle Radius

Scattering forces for varying dimensionless parameter R, the ratio of particle radius to beam waist will are presented below. Particle again is assumed to be at the beam center (X=0, Y=0, Z=0) with a laser wavelength of 1 e-6 m and laser power of 1 W. The refractive index of the particle is 1.6 and the refractive index of the medium is 1.3 with a beam waist of 10 e-6 m.

$$R = \frac{a}{w_o}$$

where

a : Particle radius, m

w_0 : Beam waist (Beam radius at focal point), m

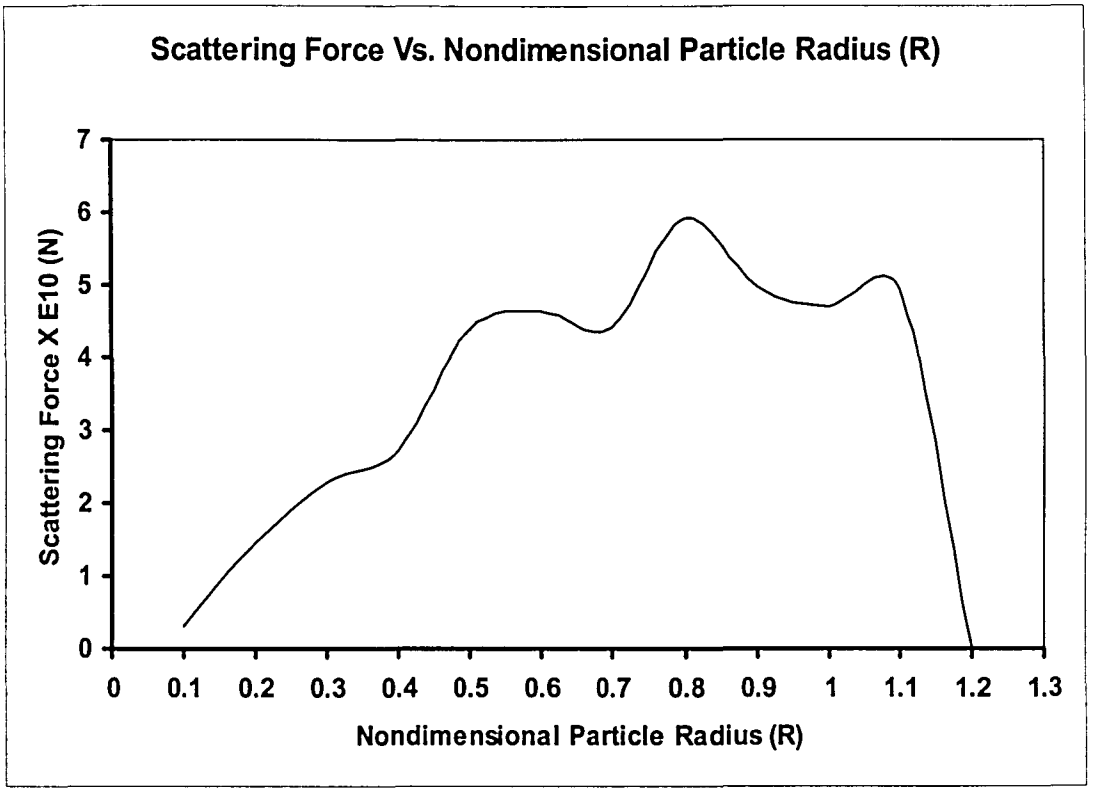

Figure 3.4 Scattering Force Vs. Nondimensional Particle Radius (R)

The GLMT theory indicates that the maximum scattering force occurs when the particle radius is about the same as the beam waist.

The fluctuations in the scattering force with increasing R are due to resonance effects. The effects of resonance on the scattering force are better explained by Nahmias [13].

3.5 Variation of Scattering Force with Refractive Index Ratio

Scattering force as a function of refractive index ratio (n), which is the ratio of particle refractive index to medium refractive index calculated using GLMT analysis is presented below. Particles are assumed to be at the beam center (X=0, Y=0, Z=0) with a laser wavelength of 1 e-6 m and laser power of 1 W. The refractive index of the medium is 1.3 with a beam waist of 10 e-6 m and particle radius of 5 e-6 m.

$$n = \frac{n_p}{n_m}$$

where

n_p : Particle refractive index

n_m : Refractive index of the medium

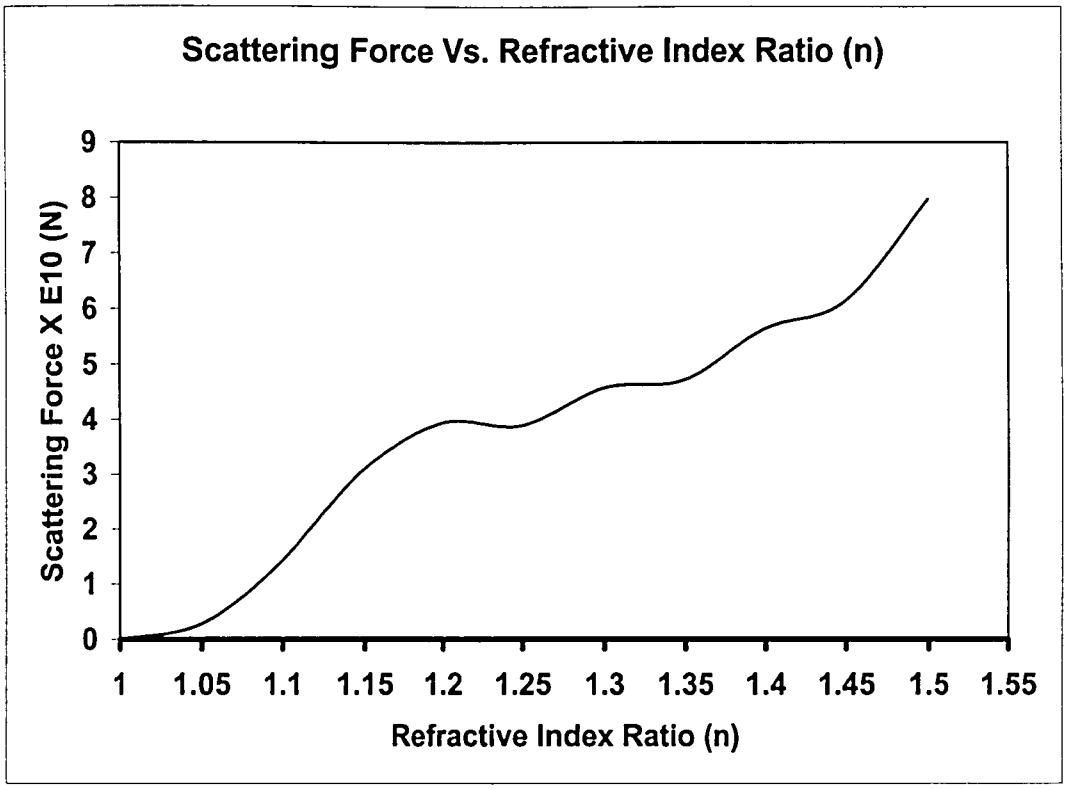

Figure 3.5 Scattering Force Vs. Refractive Index Ratio (n)

As seen from the figure and as expected from GLMT theory, scattering force seems to increase linearly with increasing n. This gives an easy way to choose the particle material. This also allows the conduct of the experiments with polystyrene particles (n_p=1.57) and prediction of the behavior with other materials such as biocells(n_p~1.4).

Chapter 4

Theory for Flow Calculations

Particles are accelerated by laser photons through a microchannel. As particles move through the channel, they transport the surrounding liquid and this is the primary pumping mechanism. The force exerted on the particles by the laser overcomes the resisting drag force on the particles.

When a particle moves through an infinite liquid medium (large liquid pool), the drag force on the particle can be calculated with Stoke's drag equations [15] as:

$$F_{\substack{Drag \\ Particle}} = 6\pi\eta a_{par} V_p \tag{4.1}$$

where

η : Viscosity of the medium, N.s/m^2

a_{par} : Radius of particle, m

V_p : Velocity of particle, m/s

If the particle moves through a channel with finite dimensions in comparison with the particle, then there will be additional drag force due to the walls of the channel [15]. These can be calculated as:

$$F_{\substack{Shear \\ Wall}} = \Delta P A_c \tag{4.2}$$

where

ΔP : Pressure drop in the microchannel, Pa

A_c : Cross sectional area of the microchannel, m^2

and

$$\Delta P = f \frac{L}{D} \rho \frac{V_\infty^{\ 2}}{2} \tag{4.3}$$

$$f = \frac{64}{\frac{\rho V_\infty D}{\eta}} \qquad \text{for low Reynolds Number Flows} \tag{4.4}$$

$$A_c = \frac{\Pi D^2}{4} \tag{4.5}$$

where

f : Friction factor, no unit

L : Length of the microchannel, m

D : Inner diameter of the microchannel, m

ρ : Density of the medium, kg/m^3

V_∞ : Average flow velocity in the microchannel, m/s

So when the particle is moving through an infinite liquid medium, the scattering force equals:

$$F_{scat.} = F_{\substack{Drag \\ Particle}} = 6\pi\eta a_{par} V_p \tag{4.6}$$

and when the particle is moving through a channel with finite dimensions, equations (4.1) and (4.2) can be combined and the scattering force equals:

$$F_{scat.} = F_{\substack{Drag \\ Particle}} + F_{\substack{Shear \\ Wall}} = 6\pi\eta a_{par} V_p + \Delta P A_c \tag{4.7}$$

When ΔP and A_c formulas are put in place, resulting equation is:

$$F_{scat.} = 6\pi\eta a_{par} V_p + 8\pi\eta L V_\infty \tag{4.8}$$

There is also another way to evaluate this type of flow (spherical particle moving in a cylindrical channel) namely Haberman Exact Theory. Here, the spherical particle is assumed to be moving along the cylindrical channel axis, the center of the channel. Total drag force on the particle can be calculated as [15]:

$$F_{\substack{Total \\ Drag}} = 6\pi\eta a_{par}(V_p K_1 - V_\infty K_2) \tag{4.9}$$

where K_1 and K_2 are wall correction factors.

Haberman Exact theory presents some tabulated values for wall correction factors for varying particle and channel diameters. These can be seen in the following table:

$\frac{a_{par}}{(D_{channel}/2)}$	K_1	K_2
0.0	1.000	1.000
0.1	1.263	1.255
0.2	1.680	1.635
0.3	2.371	2.231
0.4	3.596	3.218
0.5	5.970	5.004
0.6	11.135	8.651
0.7	24.955	17.671
0.8	73.555	43.301

Table 4.1 Wall Correction Factors (K_1 and K_2) for Haberman Exact Theory

Again, for this type of flow, scattering force exerted on the particle by the laser should account for this total drag. Thus:

$$F_{scat.} = 6\pi\eta a_{par}(V_p K_1 - V_\infty K_2) \tag{4.10}$$

As long as the scattering force can be calculated from laser and knowing particle and surrounding medium properties, velocity of the particle and the average fluid velocity in the channel can be calculated from equations (4.8) and (4.10) for different particle and channel diameters.

Chapter 5

Experimental Setup and Technique

The laser guidance system is composed of a variable power beam (TEM_{00} mode) having 1.064 μm wavelength and about 3 mm diameter before being focused. The laser is focused with a focusing lens having a numerical aperture (NA) of 0.04 and 50 mm focal length into the glass chamber as shown in figure 5.1. The glass chamber was constructed using glass cut from standard glass microscope slides of 1 mm thickness, except for the front wall, which was constructed from a glass coverslip of 100 μm thickness. The front wall was made of thinner glass to minimize the attenuation of beam. The top side of the chamber was closed with a glass slide to decrease the convection effects and to minimize the water air interaction. The overall dimensions of the flow chamber are 25 mm x 10 mm x 2 mm. The chamber is filled with deionized water.

The low numerical aperture (NA) lens was mounted on a three-axis manipulator so that the focal point of the laser beam could be located into the chamber anywhere precisely. A fused silica hollow optical fiber with a 50 μm inner diameter was used as flow tube for pumping the fluid. The fiber was kept elevated at 1 mm height using glass cut from a glass slide as indicated in the schematic. The experimental setup and the chamber are shown schematically in the following set of figures:

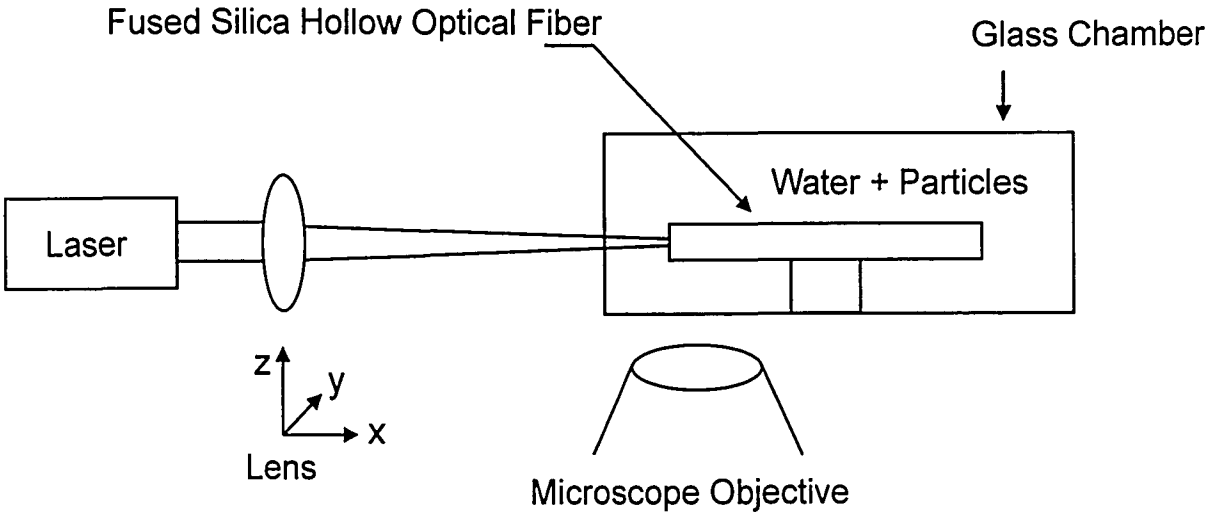

Figure 5.1 Experimental Setup

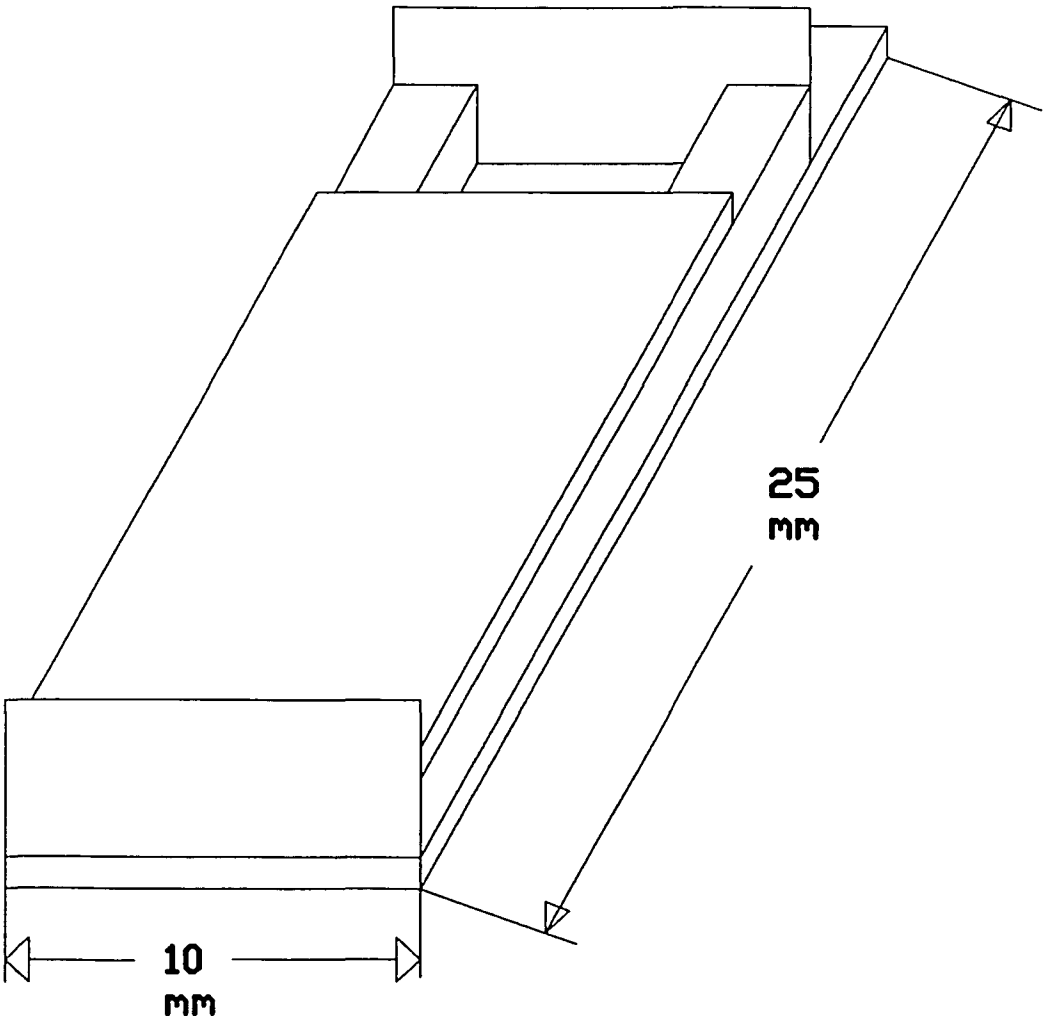

Figure 5.2 Drawing of Chamber (Top Side Closed)

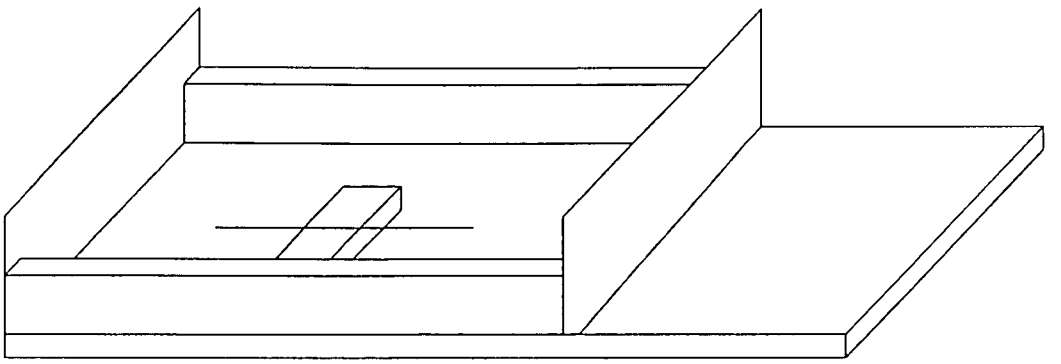

Figure 5.3 Drawing of Chamber (Top Side Open)

The IR with a wavelength of 1.064 μm (from Spectra Physics, BL-106 C Series) was focused to the chamber with a 50 mm focal length lens (Thorlabs), mounted on a 3-D (Thorlabs) manipulator. An inverted microscope (Olympus IX-70) was used in the experiment to observe the particles in the flow. A 10X, 0.3 NA Olympus UplanFI objective or a 25X, 0.5 NA Olympus UplanFI objective was used with the microscope. The flow chamber was mounted on the inverted microscope stage and the objective was mounted under the chamber. Laser light scattered by the particles was collected by the objective beneath and then projected onto a CCD camera (NEC T1-125B). The collected images were saved using an S-VHS tape-recorder (JVC HR-S9900U S-VHS). The images were then analyzed with the use of a computer program called Global Lab Image (Version 3.1, Data Translation Inc. and Acuity Imaging Ing.) to evaluate particle velocities.

In this experiment, 10 μm and 20 μm diameter polystyrene particles (from Duke Scientific Co.) were used for transporting (pumping) the demineralized distilled water through the microchannel. 1.35 μm diameter silica particles (Duke Scientific Co.), also in the fluid, were used to determine the fluid velocity in the channel since they are expected to follow the water flow better. They were also used to locate the laser beam in the chamber with light scattered from these small particles.

The particle laser interaction was first studied in the glass chamber without a microchannel. This was done to verify the validity of the methodology, the computer programs used as well as the validity of the equations used. A computer program, which is written by Nahmias [13], was used to calculate the scattering force on the particle. Global Lab Image software was used to measure the particle velocities from the experimental data. A comparison of the results is given in the next chapter.

Unfortunately, since the experimental analysis of this micropump could not be finished at this time, all experimental results will not be given in the report. Experimental results will be given in a future work.

An example of a visualization of 10μm particles with Global Lab Image software and frame grabber in 8 successive frames is shown in the following figure. Time between each of the frames is 1/30 sec. Particle velocity was determined by finding the particle location in each image and calculating the distance traveled between images. A comparison of the measured and calculated results is presented in the next chapter.

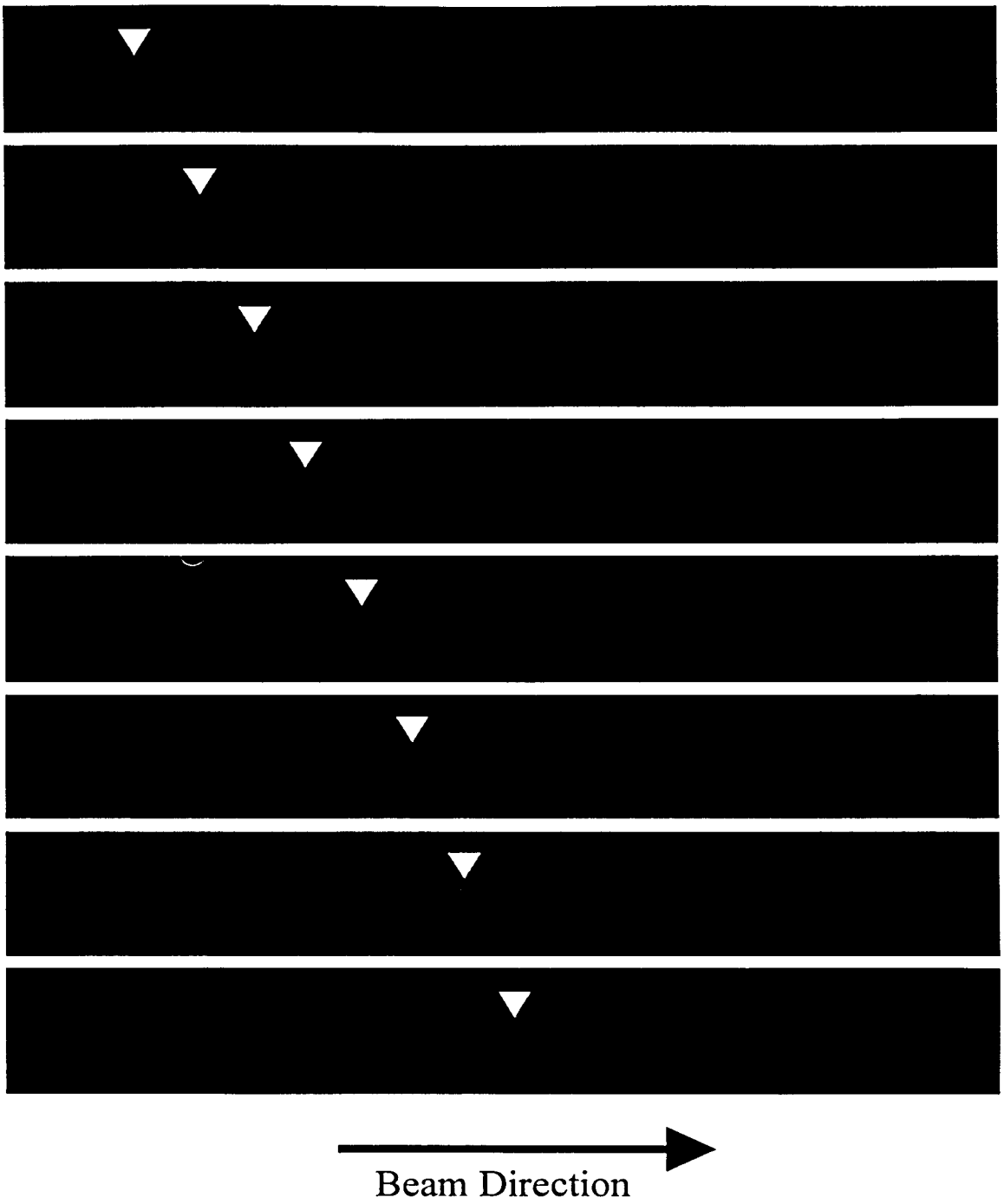

Figure 5.4 Visualization of the Motion of a 10μm Polystyrene Particle with Global Lab Image Software

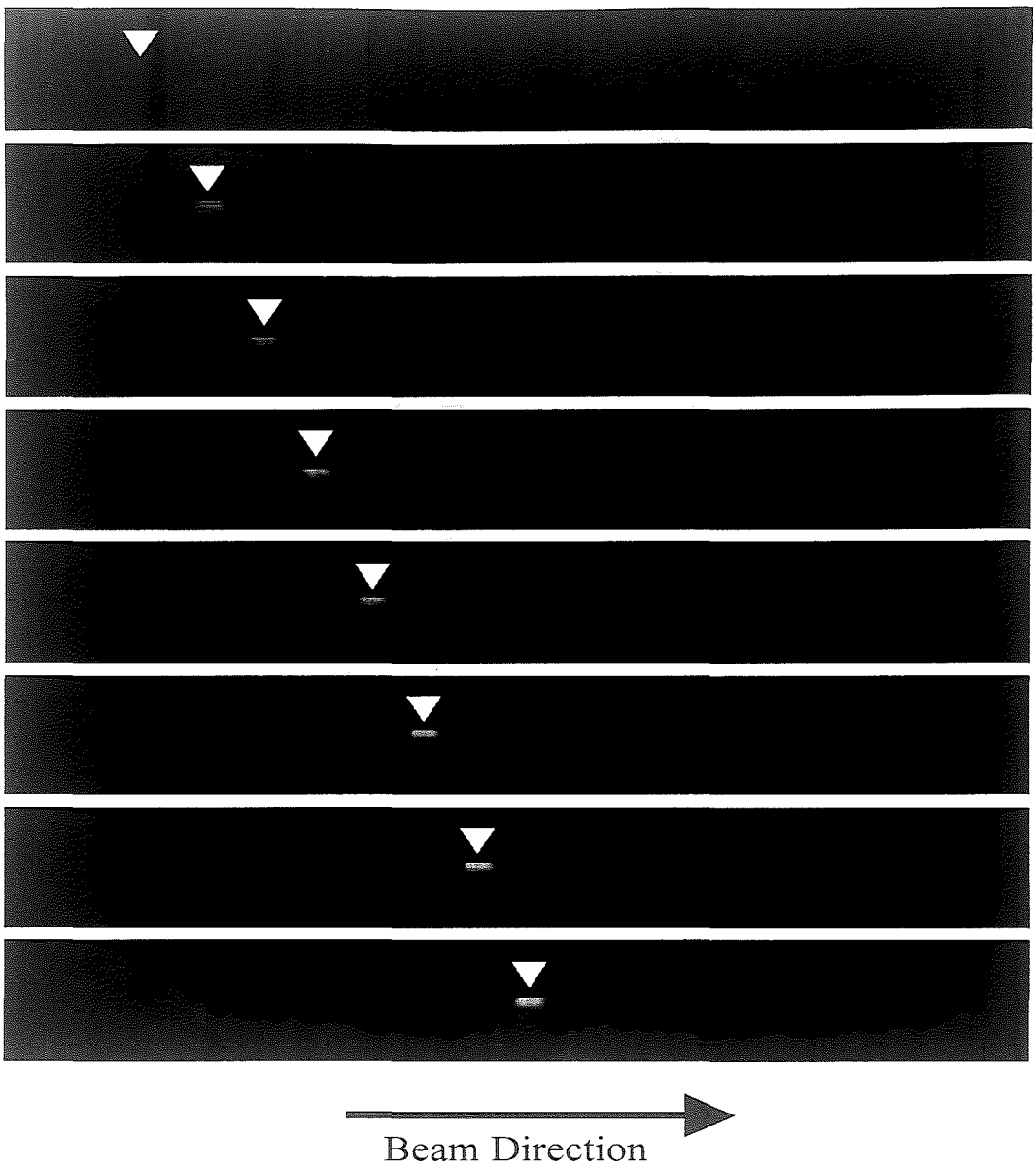

Figure 5.4 Visualization of the Motion of a 10μm Polystyrene Particle with Global Lab Image Software

Chapter 6

Comparison of Theoretical and Experimental Data

Velocity measured in the experiment are compared with those calculated using the theories presented. The analysis was performed for an experiment with the chamber without a microchannel in it. The particles thus were in an infinite fluid medium. Scattering forces on the particles were calculated using Nahmias' algoritm and also from drag force equations. Scattering force is the force component on the particle, which pushes the particle in the laser propagation direction. Gradient force is the force component, which pulls the particles to beam center. The gradient force was taken to be zero, since only the particles at the laser focal point were observed. And the theoretical calculations were performed assuming that particles are at the focal point. Scattering forces were calculated with the computer program written by Nahmias [13] and were calculated from the measured particle velocities.

6.1 Theoretical Calculations

As mentioned earlier, the scattering force on the particle was calculated with the below expression:

$$\vec{F}_{scat.}(\vec{z}) = \frac{n_m}{c}\frac{2P}{\pi(w_0)^2}\left[\hat{z}C_{pr,z}(\vec{r})\right] \tag{2.4}$$

Evaluation of $C_{pr,z}$ requires some computational techniques and the methods developed by Nahmias [13] are used.

The program calculates the scattering force as a function of location of the particle relative to beam waist center, laser wavelength, power of laser, beam radius at focal point, refractive index of particle, refractive index of medium and particle radius. Wavelength of the laser used is 1.064 μm. The calculations were performed at three different laser powers of 300 mW, 500mW and 800 mW.

Beam radius at focal point was measured to be 11 μm from the recorded images and the beam radius at focal point was calculated to be 11 μm from the following formula:

$$w_0 = (2/\pi)\lambda(f/D) \tag{6.1}$$

where

w_0 : Beam Radius at Focal Point, m

λ : Wavelength of laser, 1.064 μm

f : Focal length of lens, 50 mm

D : Beam Diameter Before Being Focused, 3 mm

Refractive indices of particle were 1.6 for silica particles and 1.57 for polystyrene particles and refractive index of medium was 1.33 for water. Particle radii were 10 μm and 20 μm for polystyrene particles and 1.35 μm for silica particles.

6.2 Experimental Data

The particles in the fluid were observed with a 10X 0.3 NA objective and a 25X 0.5NA objective through an inverted microscope. Recorded images were analyzed with the computer program (Global Lab Image). Velocities of the particles were measured at three different laser powers. From measured velocities, drag forces on the particles were calculated for Stoke's Drag for the fluid in the chamber (without a microchannel):

$$F_{\substack{Drag \\ Particle}} = 6\Pi \eta a_{par} V_p \qquad (4.1)$$

where

η : Viscosity of the medium, 1,750 e-6 N.s/m^2 for water at room temperature

Particle radii are 10 μm and 20 μm for polystyrene particles and 1.35 μm for the smaller silica particles. Particle velocities were measured at three different laser powers, 300 mW, 500mW and 800 mW.

6.3 Comparison Results

Comparison of experimental measurements with the computed results is presented in the next three figures:

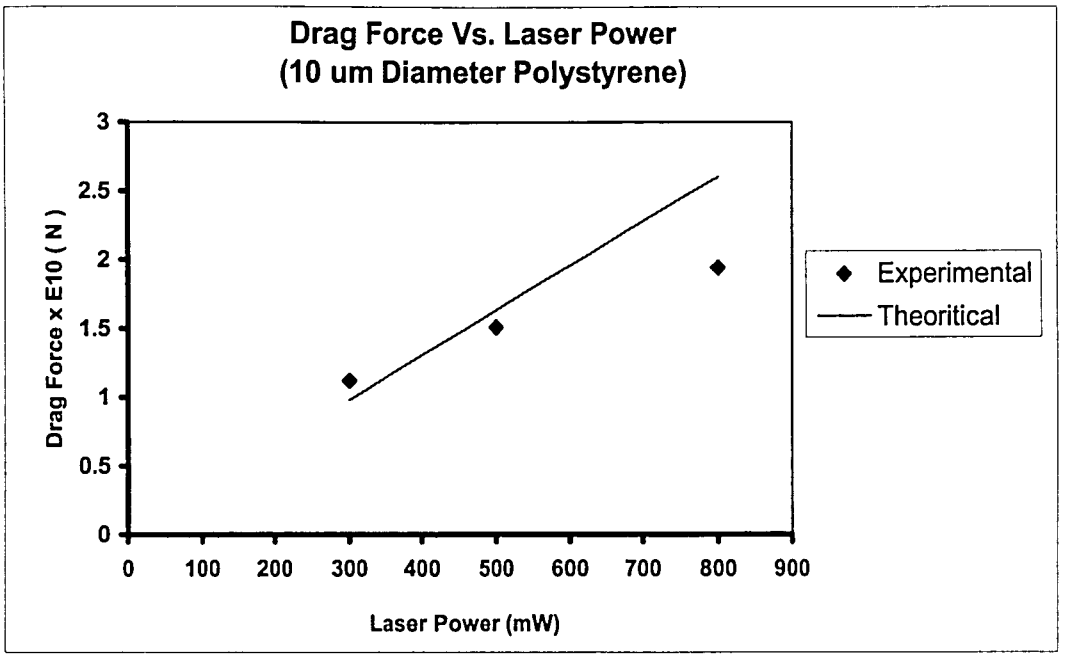

Figure 6.1 Comparison Results of 10 μm Diameter Polystyrene Particles

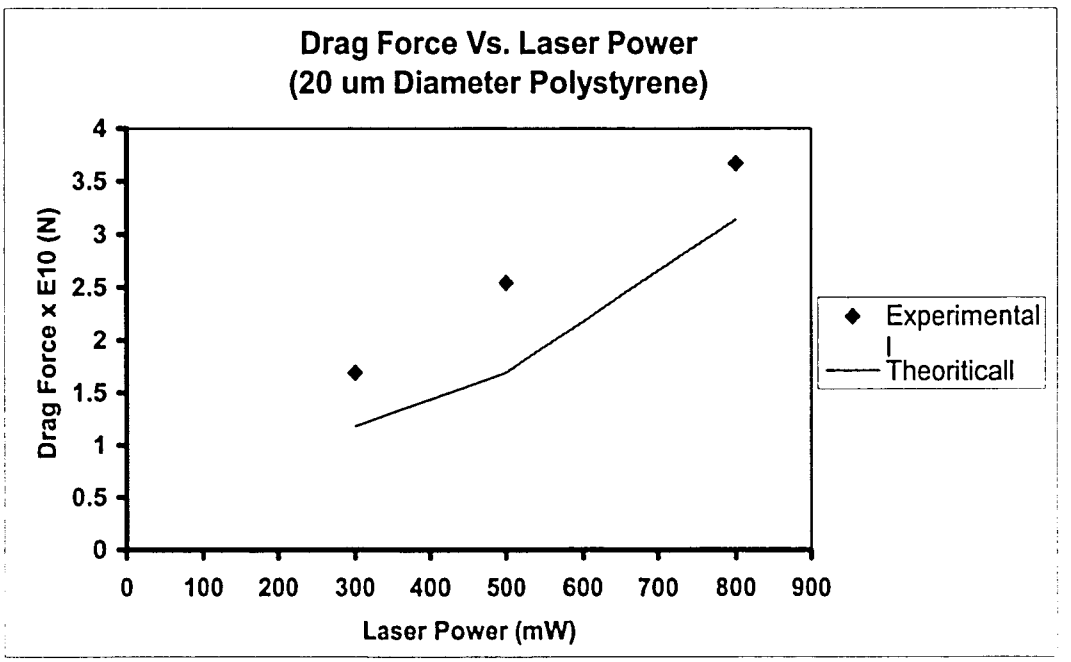

Figure 6.2 Comparison Results of 20 μm Diameter Polystyrene Particles

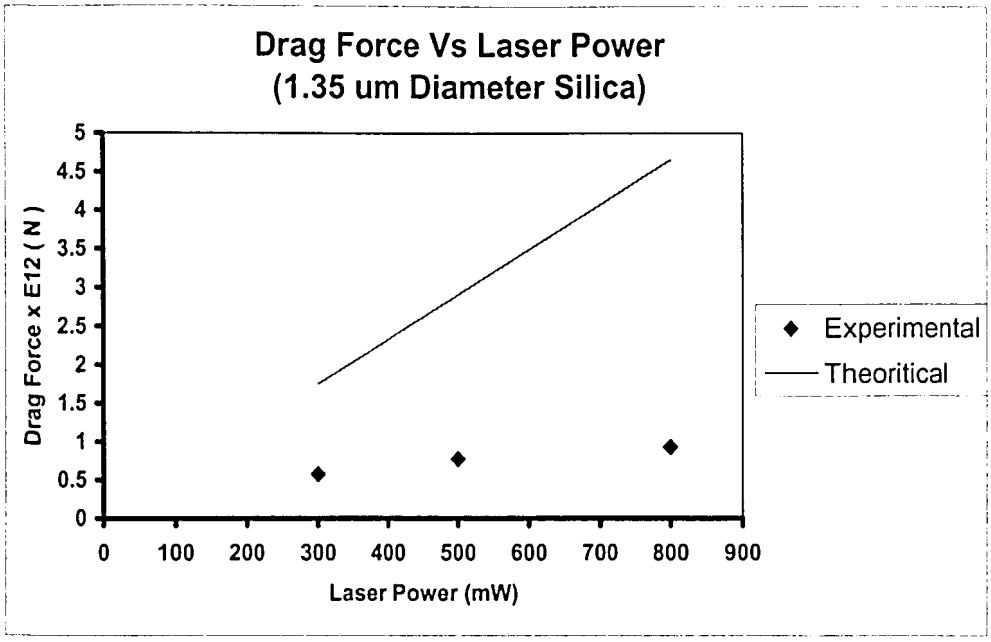

Figure 6.3 Comparison Results of 1.35 μm Diameter Silica Particles

As seen from these three figures, theoretical and experimental results are in reasonable agreement with each other for 10 μm and 20 μm diameter polystyrene particles, whereas in the results for 1.35μm silica particles the discrepancy is larger. This may be attributed to the decrease in the sensitivity of the velocity measurement as the particle size decreases.

Chapter 7

Theoretical Analysis for a Chamber with a Microchannel

As mentioned earlier, the scattering force on the particle varies with the radial location of the particle near the beam waist, diameter of the beam waist (minimal beam radius at focal point), wavelength and power of laser, beam waist, refractive index of particle, refractive index of medium and particle radius. After determinig the scattering force on the particle, it is possible to calculate the particle velocity and average fluid velocity around the particle in the microchannel (using the procedures given earlier). Particle and fluid velocities will be calculated at some fixed laser power values and for a fixed microchannel diameter in this chapter. Such an analysis forms the basis of determining the characteristics of a laser driven pump. Variations of flow in the channel can be better understood from the following figure.

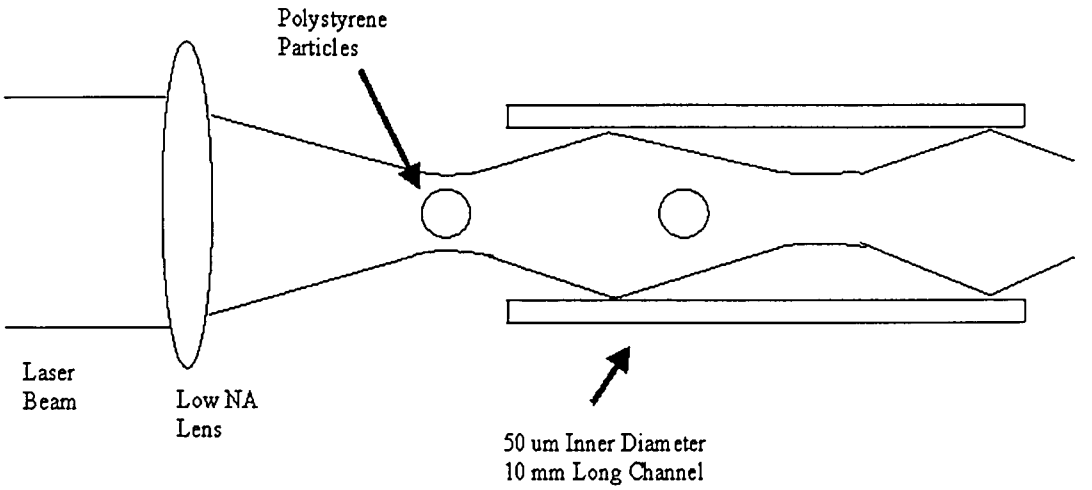

Figure 7.1 Laser Driven Micropump

Particle and fluid velocities are at different laser powers for different particle radii for particles moving in a microchannel are presented here. Particle velocities are calculated at the beam waist (X=0, Y=0, Z=0) and it is assumed that this velocity does not change through the channel. It is a reasonable assumption since the traveling in the channel, laser does not expand much in the microchannel. From the particle velocities, average fluid velocity in the channel is calculated. Laser wavelength for this experiment is 1.064 μm. Laser power is fixed at 300 mW or 500 mW or 800 mW and the beam waist is 11 μm. Particle refractive index is 1.57 for the polystyrene particles and refractive index of the medium is 1.33 for water. Particle radii are varying between 5 μm and 40 μm and the inner diameter of the channel is 50 μm and length of the channel is 10 mm. Density of water is 1,000 kg /m^3 and viscosity of water is 1,750 E-6 N.s/m^2 (at room temperature).

Following are the figures showing the variation of particle velocity, fluid velocity and flow rate with particle radius at different laser powers.

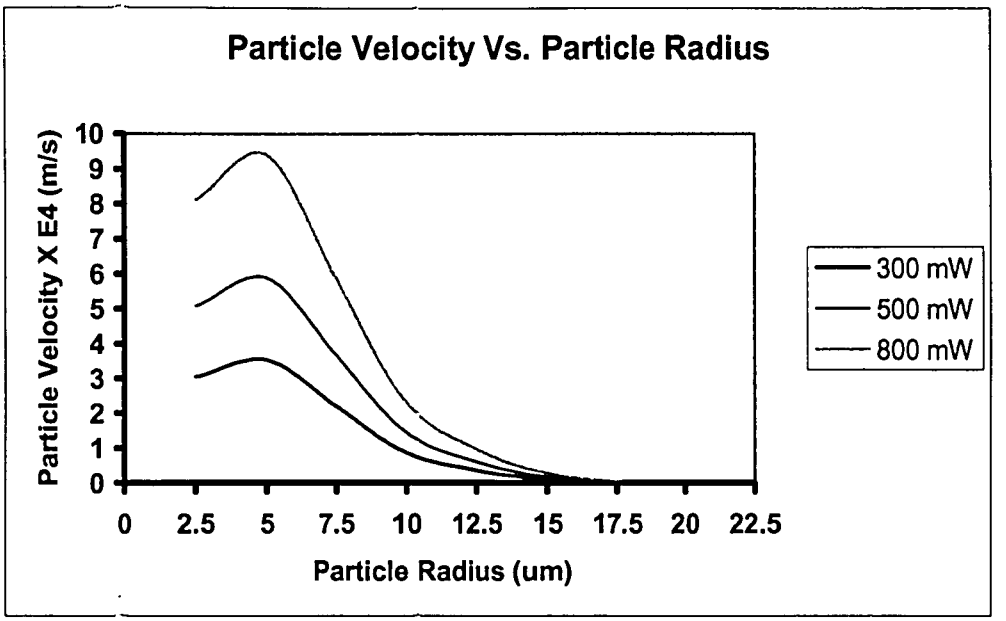

Figure 7.2: Particle Velocity Vs. Particle Radius at Different Powers for a Flow in a Microchannel

From Figure 7.2, it is seen that for this laser, optics and chamber configuration maximum particle velocity can be achieved around particle radius of 5 μm.

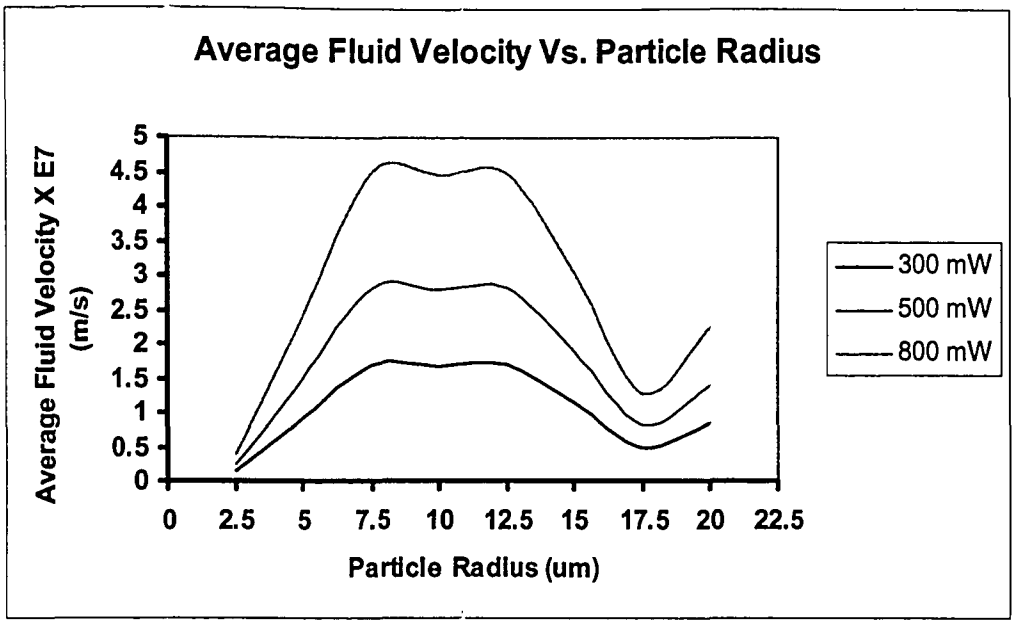

Figure 7.3 Average Fluid Velocity Vs. Particle Radius at Different Powers for a Flow in a Microchannel

From Figure 7.3, it is seen that for this laser, optics and chamber configuration maximum average fluid velocity can be achieved between particle radii of 7.5-12.5μm.

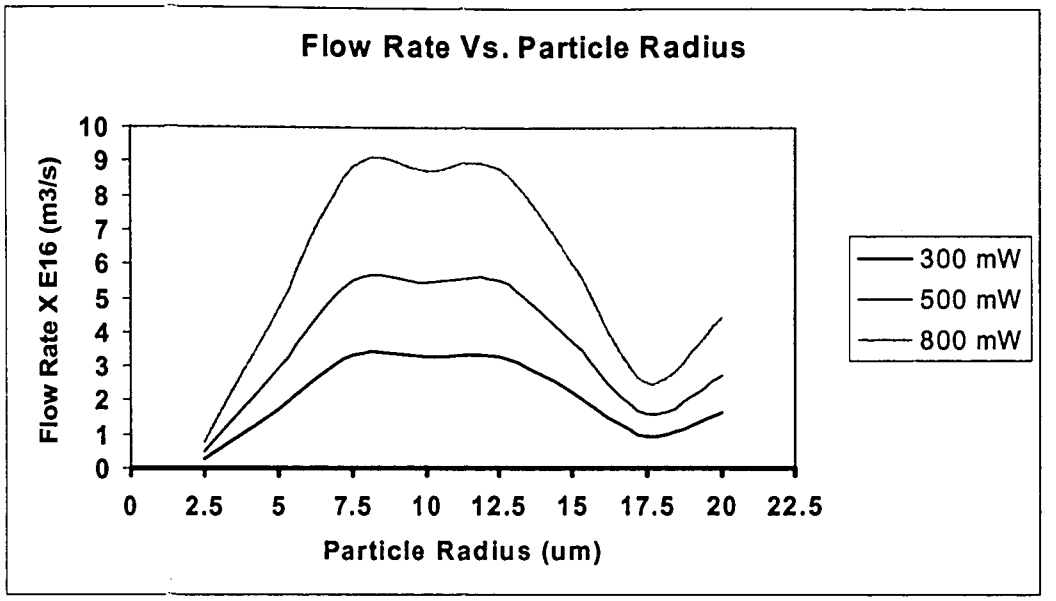

Figure 7.4 Flow Rate Vs. Particle Radius at Different Powers for a Flow in a Microchannel

From Figure 7.4, it is seen that maximum flow rate that can be achieved for this laser, optics and chamber configurations is about 10 x E-16 m^3/s corresponding to the 50 μm microchannel diameter and the velocities in Figure 7.3.

To understand the effects of drag force on the particle and drag force on the walls separately, variation of these forces at 300 mW laser power is plotted with varying particle radius.

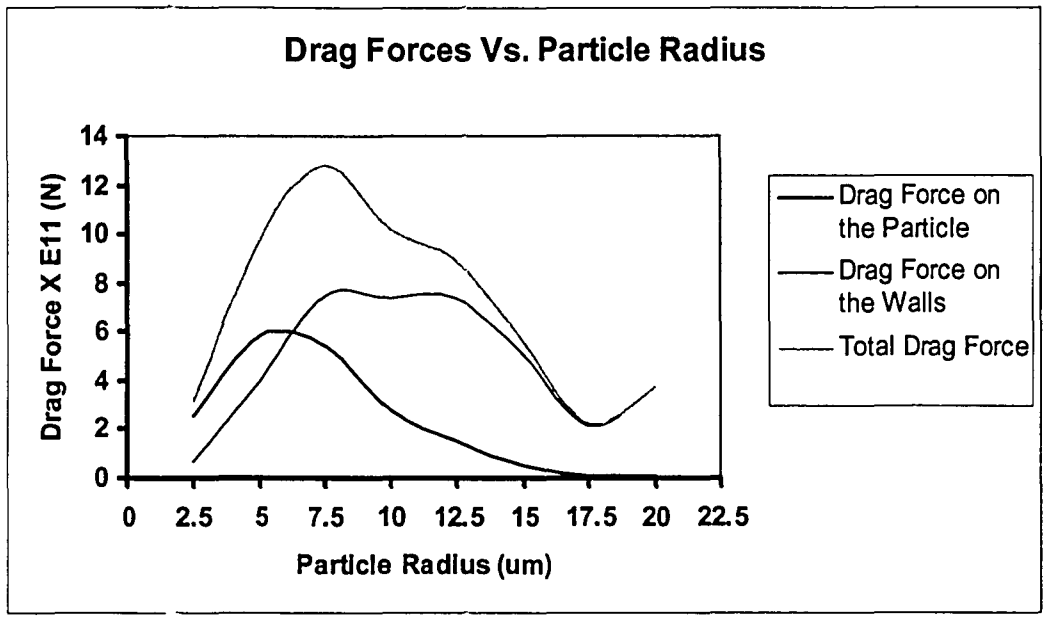

Figure 7.5 Variation of Drag force on the Particle, Drag Force on the Walls of the Microchannel and Total Drag Force with Particle Radius at 300 mW Laser Power

As particle radius increases, ratio of drag force on the particle to total drag decreases and the ratio of drag force on the walls to total drag also decreases.

CONCLUSIONS

Parametric variations for the design of a laser driven micropump have been presented. For the conditions considered here, the best particle diameter to propel fluid appears to be about 7.5 μm to 12.5 μm and the maximum flow rates can be achieved for particle to tube radius ratios of 0.3 to 0.5. Although very high flow rates cannot be achieved with this type of micropump, it has some advantages over other types of micropumps. Its simpler design, much smaller nsions and long pumping distance are the major ones. It is believed that, developing this idea further will make it possible to use this pump in biological applications where small dimensions and long pumping distance are needed.

REFERENCES

[1] S. Shoji, M. Esashi, Microflow Devices and Systems, J. Micromech. Microeng. 4 (1994) 157

[2] P. Gravesen, J. Branabjerg, O.S Jensen, Microfluidics- A Review, J. Micromech. Microeng. 3(1993) 168.

[3] A. Ashkin, History of Optical Trapping and Manipulation of Small-Neutral Particle, Atoms and Molecules, IEEE Journal on Selected Topics in Quantum Electronics, Vol. 6, No. 6, November/December 2000.

[4] A. Ashkin, Acceleration and Trapping of Particles by Radiation Pressure, Phys. Rev. Lett., Vol. 24, p 156, 1970.

[5] David J. Odde and Michael J. Renn, Laser–Guided Direct Writing For Applications in Biotechnology, Nanotechnology Journal, TIBTECH October 1999 (Vol. 17)

[6] Swadeshmukul Santra, Paul Holloway and Christopher D. Batich, Fabrication and Testing of a Magnetically Actuated Micropump, Sensors and Actuators B 87 (2002), 358-364

[7] Chuan-Hua Chen, Juan G. Santiago, A Planar Electroosmotic Micropump, Journal of Microelectromechanical Systems, Vol. 11, No. 6, December 2002.

[8] Stephen F. Bart, Lee S. Tavrow, Microfabricated Electrohydrodynamic Pumps, Sensors and Actuators, A21-A23 (1990), 193-197

[9] A. Richter, A. Plettner, K. A. Hoffmann and H. Sandmaier, A Micromachined Electrohydrodynamic (EHD) Pump, Sensors and Actuators, A29 (1991), 159-168

[10] Asuncin V. Lemoff, Abraham P. Lee, An AC Magnetohydrodynamic Micropump, Sensors and Actuators, B63 (2000), 178-185

[11] Jr-Hung Tsai and Liwei Lin, A Thermal Bubble Actuated Micronozzle Diffuser Pump, Journal of Microelectromechanical Systems, Vol.11, No. 6, December 2002

[12] A. Ashkin, Forces of a Single-Beam Gradient Laser Trap on a Dielectric Sphere in the Ray Optics Regime, Biophys. J., Vol. 61, pp 569-582. 1992

[13] Yaakov K. Nahmias and David J. Odde, Analysis of Radiation Forces in Laser Trapping and Laser-Guided Direct Writing Applications, IEEE Journal of Quantum Electronics, Vol. 38, No.2, February 2002

[14] G. Gousbet, B. Maheu, G. Grehan, Light Scattering from a Sphere Arbitrarily Located in a Gaussian Beam, Using a Bromwich Formulation, J. Opt. Soc. Am. A., Vol. 5, No. 9, September 1988.

[15] John Happel, Howard Brenner, Low Reynolds Number Hydrodynamics, 1965 by Prentice-Hall

VITA

Huseyin Cagatay Yalcin was born on April 10, 1978 in Ankara, Turkey and is the son of Mr. Yusuf Yalcin and Mrs. Hatice Yalcin. His father was a veterinarian and his mother was a civil servant and they both worked for the government. He has lived in several locations in Turkey because of his parents' jobs. He went to Anittepe High School in Ankara between 1993 and 1996. In the fall of 1996, he was accepted to Mechanical Engineering in Middle East Technical University, Ankara and graduated with a BS degree in June 2001. He received high honors student and was an honor student for several semesters. In September 2001 he started his graduate study in Mechanical Engineering and Mechanics Department, Lehigh University and is also a member of Industrial Assessment Center at Lehigh University.

END OF TITLE